European Journal of Radiology 121 (2019) 108714

Contents lists available at ScienceDirect

European Journal of Radiology

journal homepage: www.elsevier.com/locate/ejrad

Fusion Radiomics Features from Conventional MRI Predict MGMT Promoter Methylation Status in Lower Grade Gliomas

Chendan Jiang[a,1], Ziren Kong[a,1], Sirui Liu[b,1], Shi Feng[a], Yiwei Zhang[b], Ruizhe Zhu[a], Wenlin Chen[a], Yuekun Wang[a], Yuelei Lyu[b,c], Hui You[b], Dachun Zhao[d], Renzhi Wang[a], Yu Wang[a,*], Wenbin Ma[a,*], Feng Feng[b,*]

[a] Department of Neurosurgery, Peking Union Medical College Hospital, Chinese Academy of Medical Sciences and Peking Union Medical College, Beijing, China
[b] Department of Radiology, Peking Union Medical College Hospital, Chinese Academy of Medical Sciences and Peking Union Medical College, Beijing, China
[c] Department of Radiology, Beijing Chao-Yang Hospital, Capital Medical University, Beijing, China
[d] Department of Pathology, Peking Union Medical College Hospital, Chinese Academy of Medical Sciences and Peking Union Medical College, Beijing, China

ARTICLE INFO

Keywords:
Radiomics
MRI
MGMT promoter methylation
Lower grade glioma
Fusion

ABSTRACT

Purpose: The methylation status of the O6-methylguanine-DNA methyltransferase (*MGMT*) promoter has been proven to be a prognostic and predictive biomarker for lower grade glioma (LGG). This study aims to build a radiomics model to preoperatively predict the *MGMT* promoter methylation status in LGG.

Method: 122 pathology-confirmed LGG patients were retrospectively reviewed, with 87 local patients as the training dataset, and 35 from The Cancer Imaging Archive as independent validation. A total of 1702 radiomics features were extracted from three-dimensional contrast-enhanced T1 (3D-CE-T1)-weighted and T2-weighted MRI images, including 14 shape, 18 first order, 75 texture, and 744 wavelet features respectively. The radiomics features were selected with the least absolute shrinkage and selection operator algorithm, and prediction models were constructed with multiple classifiers. Models were evaluated using receiver operating characteristic (ROC).

Results: Five radiomics prediction models, namely, 3D-CE-T1-weighted single radiomics model, T2-weighted single radiomics model, fusion radiomics model, linear combination radiomics model, and clinical integrated model, were built. The fusion radiomics model, which constructed from the concatenation of both series, displayed the best performance, with an accuracy of 0.849 and an area under the curve (AUC) of 0.970 (0.939-1.000) in the training dataset, and an accuracy of 0.886 and an AUC of 0.898 (0.786-1.000) in the validation dataset. Linear combination of single radiomics models and integration of clinical factors did not improve.

Conclusions: Conventional MRI radiomics models are reliable for predicting the *MGMT* promoter methylation status in LGG patients. The fusion of radiomics features from different series may increase the prediction performance.

1. Introduction

Glioma accounts for 75% of malignant primary central nervous system (CNS) tumors but suffers an unfavorable prognosis despite surgical excision, chemotherapy, and radiotherapy[1]. O^6-methylguanine-DNA methyltransferase (MGMT) is a DNA repair enzyme that removes the guanine-alkyl group induced by alkylating agents such as temozolomide (TMZ)[2]. The methylation of the *MGMT* promoter,

Abbreviations: 3D-CE-T1-weighted, three-dimensional contrast enhanced T10-weighted; AUC, area under curve; CNS, central nervous system; SD, standard deviation; LASSO, least absolute shrinkage and selection operator; LGG, lower grade gliomas, which refers to WHO grade II and III gliomas; MGMT, O6-methylguanine-DNA methyltransferase; MRI, magnetic resonance imaging; PCR, polymerase chain reaction; PFS, progression-free survival; ROI, region of interest; ROC, receiver operating characteristic; SVM, support vector machine; TCGA, The Cancer Genome Atlas; TCIA, The Cancer Imaging Archive; TMZ, temozolomide; WHO, World Health Organization

* Corresponding authors at: Peking Union Medical College Hospital (East), No. 1 Shuaifuyuan Wangfujing Dongcheng District, Beijing, China.
E-mail addresses: jiangchendan@gmail.com (C. Jiang), kongziren@pumc.edu.cn (Z. Kong), lsr0303@126.com (S. Liu), joule_feng@163.com (S. Feng), zhangyiweilucy@126.com (Y. Zhang), zhu.rui.zhe@163.com (R. Zhu), cwl2014thupumc@126.com (W. Chen), skafear@yeah.net (Y. Wang), lyl0211@163.com (Y. Lyu), you_hui@hotmail.com (H. You), dachunzhao@126.com (D. Zhao), wangrenzhi@pumch.cn (R. Wang), ywang@pumch.cn (Y. Wang), mawb2001@hotmail.com (W. Ma), ffeng@pumch.cn (F. Feng).
[1] These authors contributed equally to this work.

https://doi.org/10.1016/j.ejrad.2019.108714
Received 27 May 2019; Received in revised form 5 September 2019; Accepted 13 October 2019

which epigenetically silences the *MGMT* gene, has become a strong prognostic and predictive biomarker of World Health Organization (WHO) grade II, III and IV gliomas[3–5]. Therefore, measurement of *MGMT* promoter methylation status has been widely applied in the clinical evaluation of glioma patients. However, the *MGMT* promoter status is mainly determined by methylation-specific polymerase chain reaction (PCR), pyrosequencing or a methylation chip[2,6,7] based on a tumor sample, which is hindered by the relatively long detection period, the tumor heterogeneity and the unavailability of surgery or biopsy. Thus, preoperatively and noninvasively evaluating the *MGMT* promoter methylation status is of great clinical significance.

Magnetic resonance imaging (MRI) is routinely applied in the initial evaluation of gliomas, and early studies have investigated the association between MRI characteristics and *MGMT* promoter methylation status[8–10]. Recent advances in radiomics allow a quantitative description of tumor characteristics with high-throughput radiomics features extracted from imaging data and the establishment of a predictive model to predict the tumor phenotype through selected features[11]. In the field of glioma research, several MRI-based radiomics studies have demonstrated the correlation of MRI radiomics features with glioma WHO grading[12,13], molecular characteristics[14–17], clinical manifestations[18], and patients' prognosis[19,20].

Although promising results have been revealed with the use of radiomics to predict glioma features, limited studies have focused on predicting *MGMT* promoter methylation status[21–23]. In particular, Li et al. and Xi et al. investigated radiomics models of glioblastoma [21,22], and Wei et al. explored the radiomics features of WHO grade II-IV astrocytomas[23]; however, none of these studies specifically focused on lower grade gliomas (LGG, which refers to WHO grade II and III gliomas). Since recent studies have suggested that the *MGMT* promoter methylation status is an independent prognostic biomarker of WHO grade II and WHO grade III gliomas and a predictive biomarker for the response to alkylating agents regardless of histological classification[3,4,24,25], radiomics prediction of *MGMT* promoter methylation status may have great potential in clinical practice.

This study retrospectively investigated the imaging characteristics from pretreatment conventional MRI images of LGGs using a radiomics approach, aiming to build a reliable model to noninvasively predict the *MGMT* promoter methylation status in LGG patients.

2. Materials and Methods

2.1. Patients

This study retrospectively reviewed patients with pathologically confirmed LGG treated at our hospital between August 2010 and March 2018. The inclusion criteria were as follows: 1) adults with histopathology confirmed primary WHO grade II and III gliomas with no previous history of CNS tumors; 2) frozen tumor tissues available for the measurement of *MGMT* promoter methylation status; 3) preoperative MRI examination including three-dimensional contrast enhanced T1 (3D-CE-T1)-weighted imaging and T2-weighted imaging; and 4) no radiotherapy, chemotherapy or other therapy delivered before MRI acquisition and surgery. The study design and protocol were approved by the Institutional Review Board, and all patients provided informed consent. Imaging data from the open-access database The Cancer Genome Atlas Low Grade Glioma (TCGA-LGG) data collection, hosted on The Cancer Imaging Archive (TCIA) which met the inclusion criteria 1), 3), and 4) and had available *MGMT* promoter methylation status, were also acquired (www.cancerimagingarchive.net). Finally, a total of 87 local patients met the inclusion criteria and were assigned into a training dataset, and 35 patients from the TCIA-LGG dataset were included as an independent validation dataset. The recruitment pathway of the involved patients is shown in Fig. 1.

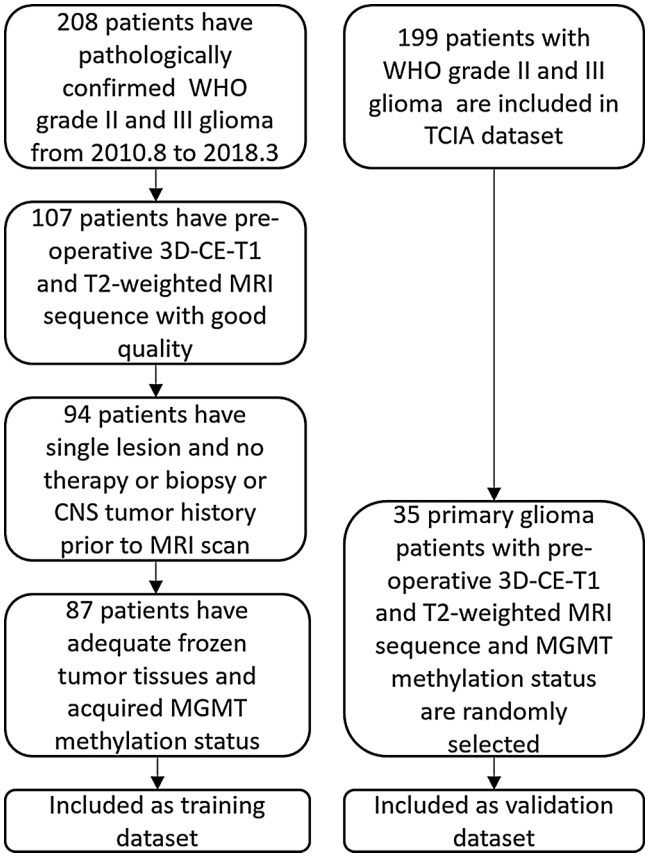

Fig. 1. Local patients were recruited to the training dataset, and patients from The Cancer Imaging Archive (TCIA) were recruited to the validation dataset.

2.2. Measurement of the MGMT Promoter Methylation Status

The *MGMT* promoter methylation status of the local patients was measured by pyrosequencing as described by Reifenberger et al[26]. DNA was extracted from frozen tumor tissues using a Simlex OUP®FFPE DNA extraction kit (TIB, China) and subsequently quantified by spectrophotometry using a NanoDrop 2000 (Thermofisher, US). Bisulfate modification was carried out using an EpiTect Bisulfite Kit (Qiagen, Germany). PCR was accomplished with a DRR007 kit (Takara, Japan) using the Verity 96-Well Thermal Cycler (Thermofisher, US), and pyrosequencing was performed using the PyroMark Q96 system (Qiagen, Germany) in 10 CpG island region within the *MGMT* promoter. Glioma was defined as 'methylated' if the average methylation rate of the CpG regions ≥ 8%, otherwise the tumor was recognized as 'unmethylated' [26].

2.3. MRI Data Acquisition and Preprocessing

Preoperative MRI of the local patients was performed on a 3.0-T MRI scanner (Discovery MR750, GE, US). The MRI protocol included 3D-CE-T1-weighted images (repetition time, 6.2-8.3 ms; echo time, 2.6-3.2 ms; inversion time, 400 ms; slice thickness, 1 mm; matrix, 256 × 256) and T2-weighted images (repetition time, 3440-4060 ms; echo time, 85-103 ms; slice thickness, 5-6 mm; matrix, 256 × 256). 3D-CE-T1-weighted images were obtained after the injection of 0.1 mmol/kg of gadolinium chelate contrast medium. All MRI images were automatically interpolated to a 512 × 512 resolution by the MRI system. All of the DICOM data acquired from the MRI scanner were converted to NIfTI formats for later processing, and the patient information was simultaneously removed for privacy purposes.

2.4. Image Segmentation

T2-weighted images were co-registered to the 3D-CE-T1-weighted images to delimit the tumor boundaries as well as to eliminate the influence of head movement on tumor features in the same patient. Tumors were then manually segmented by two experienced neurosurgeons who were blinded to the patients' information using the ITK-SNAP software (http://www.itksnap.org/pmwiki/pmwiki.php). Both 3D-CE-T1-weighted and T2-weighted series were referred during the segmentation. The three-dimensional region-of-interest (ROI) mask, which included contrast-enhancement region for contrast-enhanced tumor and the abnormal T2 signals for the non-contrast-enhanced tumor, was delineated on 3D-CE-T1-weighted images (exampled in Supplementary material 1) and co-registered to T2-weighted images with FSL (Functional Magnetic Resonance Imaging of the Brain Analysis Group, Oxford University, UK [FMRIB] Software Library) [27–29] to avoid inconsistencies in ROIs between different imaging sequences. The ROI mask was subsequently reevaluated by a senior neuro-radiologist to ensure the quality. If the discrepancies of ROI ≤ 5% between the two neurosurgeons, the final ROI was defined as the overlapping area of their segmentations; if the discrepancies of ROI > 5%, the neuro-radiologist made the final decision.

2.5. Postprocessing and Feature Extraction

Normalization of the brightness level was performed on 3D-CE-T1 and T2-weighted images with a preset module in pyradiomics (2.1.0, http://www.radiomics.io/)[30], which normalizes the image by centering it at the mean with standard deviation based on all gray values in the image. A total of 1702 radiomics features were extracted with pyradiomics[30], including 14 shape features, 18 first order features, 75 texture features (derived from GLCM, GLRLM, GLSZM, GLDM, and NTGDM), and 744 wavelet features. The extracted features are summarized in Supplementary material 2 and detailed in Supplementary material 3.

2.6. Feature Selection and Model Construction

All of the data were normalized with a scaler based on the standard deviation (SD) of the training dataset to minimize the influence of data fluctuations on the classifiers, and the identical scaler with parameters of the training dataset was also applied to the validation dataset. The features were selected with the least absolute shrinkage and selection operator (LASSO)[31], and the code was constructed with Scikit-learn (v0.20.0, http://scikit-learn.org).[32] The default alpha value of the elastic-net penalty function was lowered down to 1.0×10^{-7} in the LASSO model to ensure that more available related features could be included in the model. Multiple selection thresholds were evaluated to find the optimum setting for all radiomics features[33]. All of the features had equal priority before selection. The prediction model was constructed with multiple classifiers including a standard support vector machine (SVM) classifier, a random forest classifier, and an AdaBoost classifier with a decision tree or SVM as the base classifier. The model was trained with our local radiomics data.

Five radiomics prediction models, namely, 3D-CE-T1-weighted single radiomics model, T2-weighted single radiomics model, fusion radiomics model, linear combination radiomics model, and clinical integrated model, were built.

Radiomics features extracted from 3D-CE-T1 and T2-weighted series were selected and used for model construction separately as single radiomics predictors.

These optimized single models were linearly combined as a new linear combination radiomics predictor. The prediction value of the model was defined as follows with a coefficient value:

$$Signature_{Linear-combination} = k \bullet Signature_{3D-T1-CE} + (1 - k) \bullet Signature_{T2}$$

The fusion radiomic model was based on the selected features from both of the 3D-CE-T1 and T2-weighted modalities, instead of respectively selection. All of the 1702 features were concatenation together, and *de novo* selection were performed instead of combining the selected features. The classification was performed on selected features.

The clinical integrated prediction model shared the same features with the fusion radiomics model, with age appended as a new feature.

2.7. Model Validation

The predictive models were validated on the independent validation cohort constructed with the TCIA-LGG data. The performance was assessed using accuracy, sensitivity, specificity and area under the receiver operating characteristic (ROC) curve (AUC). The DeLong method was used for statistical comparison of the ROC curves and calculation of the confidence interval of the AUC[34].

The patients whose *MGMT* promoter methylation status was correctly predicted were selected to generate the radiomics maps, aiming to illustrate regional differences between patients with positive and negative *MGMT* methylation status.

2.8. Statistical Analysis

All statistical analyses were performed with R 3.4.1 (https://www.r-project.org) and Python 3.6.5 (https://www.python.org). ROC analysis was done with the package pROC. For the calculation of the confidential interval of the AUC and the Z- scores, DeLong method was used.

3. Results

3.1. Patient Characteristics and Molecular Subtype

The baseline characteristics of the 122 included patients are detailed in Table 1. No significant difference in patients' clinical characteristics was observed in the training cohort (n = 87) and validation cohort (n = 35). The training and validation cohorts contained 60 (69.0%) and 28 (80.0%) patients, respectively, with *MGMT* promoter methylation, and 27 (31.0%) and 7 (20.0%) patients, respectively, without *MGMT* promoter methylation, and no significant difference was shown in the distribution of *MGMT* methylation status (p = 0.268). For the distribution of *IDH* mutation status in *MGMT* promoter methylation positive and negative patients, no significant difference were shown between the training and validation cohorts (p = 0.100 and 0.186 respectively).

Table 1
Patient Characteristics of the Training Cohort and Validation Cohort.

Characteristics	Training Cohort	Validation Cohort	P-value
Sex			0.691
Male	43 (49.4%)	19 (54.3%)	
Female	44 (50.6%)	16 (45.7%)	
Age (Mean ± SD)	45.4 ± 13.1	44.2 ± 15.7	0.678
MGMT			0.268
Methylated	60 (69.0%)	28 (80.0%)	0.100
IDH(+)	43 (71.7%)	25 (89.3%)	
IDH(-)	17 (28.3%)	3 (10.7%)	
Unmethylated	27 (31.0%)	7 (20.0%)	0.186
IDH(+)	7 (25.9%)	4 (57.1%)	
IDH(-)	19 (70.4%)	3 (42.9%)	
Unknown	1 (3.7%)	0 (0.0%)	
WHO Grade			0.545
Grade II	48 (55.2%)	22 (62.9%)	
Grade III	39 (44.8%)	13 (37.1%)	

Notes: Unless otherwise noted, data in the table refers to the number of patients, with percentages in parentheses.

Table 2
Detail of the Selected Features in Fusion Radiomics Model.

No.	Feature Name	Modality	Matrix	Processing	Type
F1	Large Dependence High Gray Level Emphasis	3D-CE-T1-weighted	GLDM	Original	Texture
F2	IMC2	3D-CE-T1-weighted	GLCM	Wavelet-LLH	Wavelet Texture
F3	Maximum	3D-CE-T1-weighted	First Order	Wavelet-LHH	Wavelet Intensity
F4	Skewness	3D-CE-T1-weighted	First Order	Wavelet-LHH	Wavelet Intensity
F5	Large Area High Gray Level Emphasis	T2-weighted	GLSZM	Wavelet-LLH	Wavelet Texture
F6	Large Area Low Gray Level Emphasis	T2-weighted	GLSZM	Wavelet-LHL	Wavelet Texture
F7	Zone Entropy	T2-weighted	GLSZM	Wavelet-LHL	Wavelet Texture
F8	Median	T2-weighted	First Order	Wavelet-LHH	Wavelet Intensity
F9	IDN	T2-weighted	GLCM	Wavelet-HLL	Wavelet Texture
F10	Cluster Prominence	T2-weighted	GLCM	Wavelet-HLH	Wavelet Texture
F11	Difference Entropy	T2-weighted	GLCM	Wavelet-HLH	Wavelet Texture
F12	IMC1	T2-weighted	GLCM	Wavelet-HHL	Wavelet Texture
F13	Joint Average	T2-weighted	GLCM	Wavelet-HHH	Wavelet Texture
F14	High Gray Level Zone Emphasis	T2-weighted	GLSZM	Wavelet-HHH	Wavelet Texture
F15	Size Zone Non Uniformity	T2-weighted	GLSZM	Wavelet-HHH	Wavelet Texture

Notes: The original image is decomposed into 8 wavelet decompositions, by low-pass (L) and high-pass (H) filtering in three directions.
Abbreviations: 3D-CE-T1-weighted, three-dimensional contrast enhanced T1-weighted; GLCM, Gray-Level Co-occurrence Matrix; GLSZM, Gray Level Size Zone Matrix; IMC, Informational Measure of Correlation; IDN, Inverse Difference Normalized.

3.2. Feature Selection

Multiple possible feature combinations had the potential to construct good classifiers for distinguishing *MGMT* status. Fifteen features were selected for the fusion radiomics model with stable order as the desired number of features increased (detailed in Table 2), and 19 features were selected for each single radiomics model (detailed in Supplementary material 4). The same feature set from the fusion radiomics model was also utilized in the clinical integrated model, with patient age as an independent feature. Clustered heatmaps of all radiomics features and selected features of the fusion radiomics model were demonstrated in Supplementary material 5.

3.3. Model Validation and Model Comparison

The performance of each prediction model in the training and validation datasets is detailed in Table 3, and the ROC curve for all the prediction models in the training and validation datasets is displayed in Fig. 2a and b. In short, the AUCs of the 5 radiomics prediction models ranged from 0.873 (0.795-0.952) to 0.970 (0.939-1.000) in the training dataset, and 0.745 (0.456-1.000) to 0.898 (0.786-1.000) in the validation dataset (Table 3). The prediction models demonstrated relatively good accuracy and balanced sensitivity and specificity. The optimized prediction model, fusion radiomics model, showed an accuracy of 0.840 and an AUC of 0.970 in the training dataset, and an accuracy of 0.886 and an AUC of 0.898 in the validation dataset Bar charts for the fusion radiomics model and other prediction models are displayed in Fig. 2c, d and Supplementary material 6. The radiomics feature maps of the selected features in the fusion radiomics model are shown in Fig. 3.

The coefficient of the linear combination radiomics model was determined as follows:

$$Signature_{Linear-combination} = k \bullet Signature_{3D-T1-CE} + (1 - k) \bullet Signature_{T2},$$

where $k = 0.02$ *in our optimized model*

The linear combination radiomics model showed an AUC of 0.881 in the training dataset and 0.745 in the validation dataset, and the performance of this model in the training dataset was not inferior to that of any of the two single radiomics predictors. Clinical information, the age of the patients, was first added as an independent feature to the extracted high-throughput radiomics was not chosen by the LASSO selector, which picks features with the highest 30 weights, but the algorithm became very hard to converge on the training dataset with approximately 30 features. Forcibly appending age information into the fusion radiomics model (that is, the clinical integrated model) did not lead to superiority of the model over the fusion radiomics feature-based prediction model.

When comparing the performance between each model, the fusion radiomics model and the clinical radiomics model showed no statistical difference ($p = 0.967$) in the training dataset, and they were significantly different from the other predictors ($p = 0.0152$-0.0213). The ROCs of the single radiomics model and the linear radiomics model showed no statistic differences in the training dataset. In the validation dataset, the fusion model and the clinical model did not show statistical differences with the other models. The Z-scores between the fusion model, the clinical model and the other models ranged from 0.872 to 1.271.

4. Discussion

In this study, *MGMT* promoter methylation status-related 3D-CE-T1 and T2-weighted MRI radiomics features were selected and analyzed using local data and validated using TCIA data. Five radiomics

Table 3
Prediction Performance of Five Radiomics Model.

Models	Training Cohort				Validation Cohort			
	ACC	SEN	SPE	AUC (95% CI)	ACC	SEN	SPE	AUC (95% CI)
3D-CE-T1 Single Model	0.839	0.750	0.815	0.873 (0.795-0.952)	0.886	0.714	0.714	0.804 (0.570-1.000)
T2-weighted Single Model	0.805	0.783	0.815	0.879 (0.807-0.951)	0.800	0.821	0.714	0.760 (0.516-1.000)
Linear Combination Model	0.805	0.800	0.778	0.881 (0.810-0.951)	0.882	0.929	0.714	0.745 (0.456-1.000)
Fusion Radiomics Model	0.839	0.883	0.926	0.970 (0.939-1.000)	0.886	0.821	0.857	0.898 (0.786-1.000)
Clinical Integrated Model	0.839	0.889	0.917	0.969 (0.939-1.000)	0.886	0.929	0.714	0.811 (0.616-1.000)

Abbreviations: 3D-CE-T1, three-dimensional contrast enhanced T1-weighted; ACC, accuracy; SEN, sensitivity; SPE, specificity; AUC, area under curve; CI, confidence interval.

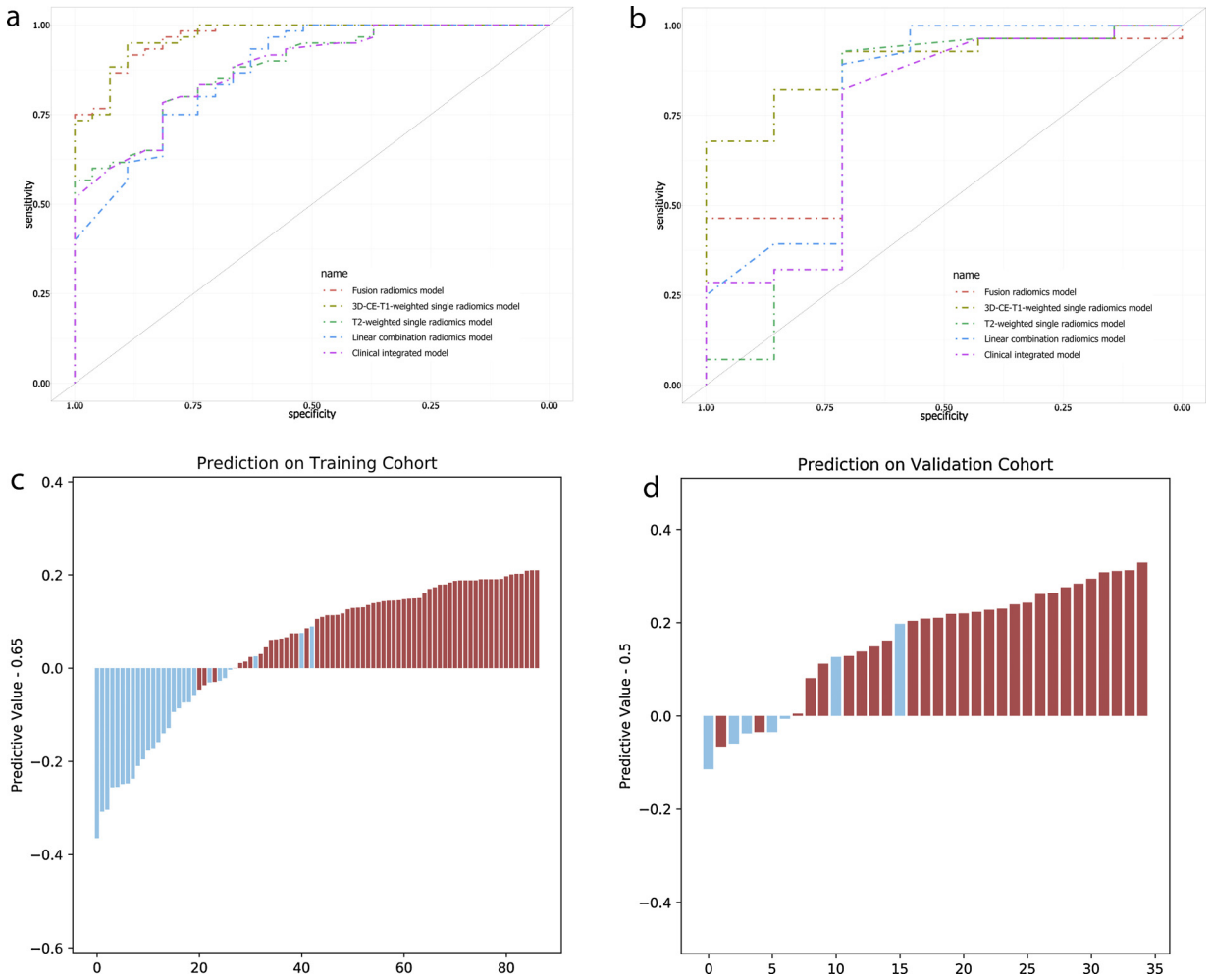

Fig. 2. Receiver operating characteristic (ROC) curve was utilized to evaluate the performance of the 5 radiomics prediction model in training cohort (a) and validation cohort (b). Bar charts was applied to demonstrate the performance of fusion radiomics model in training cohort (c) and validation cohort (d). The red bars with the predictive value minus threshold > 0 and the blue bars with the predictive value minus threshold < 0 indicate the successful classification of the prediction model, and vice versa.

prediction models that could predict *MGMT* promoter methylation status in LGG were constructed, and the fusion radiomics model displayed the best performance. The study results demonstrated a conventional MRI radiomics-based method to evaluate *MGMT* status in LGG patients, and the fusion of radiomics features from different imaging series may improve the performance of the prediction model.

Previous studies on noninvasive *MGMT* promoter methylation prediction have mainly investigated visually assessed features (e.g., tumor location, tumor border, image texture, edema that evaluated by radiologist)[8–10] or machine-learning selected radiomics features[21–23] of multimodality MRI images of gliomas, and the accuracy of these predictions (in the validation dataset) ranged from 0.58-0.80, while the AUC ranged from 0.75-0.90. However, previous radiomics studies mainly predicted the *MGMT* promoter methylation status of glioblastomas[21,22] or WHO grade II-IV astrocytomas[23], and to the best of our knowledge, out study is the first to explorer the *MGMT* status of WHO grade II and III gliomas using a radiomics approach. Our prediction model with fusion of 3D-CE-T1 and T2-weighted features demonstrated a higher accuracy and comparable AUC value compared with models of previous studies, indicating the strong potential of radiomics to predict the *MGMT* status in LGG patients. A major reason for the excellent performance of our model may be the fusion of features from different series of conventional MRI images, where T2-weighted features offer distinguishable information and 3D-CE-T1-weighted features provide higher accuracy in representing tumor characteristics thanks to the added value of gadolinium, thin slice thickness (1 mm) and three-dimensional reconstruction of images (in comparison, the section thickness of previously reported MRI data was usually 4.0-5.0 mm[21–23]). In addition, most radiomics models were trained and validated with single-center data, yet our study was validated with data from TCIA, which were acquired from multiple centers with different equipment under various conditions, suggesting the generalizability of our model. However, TCIA data has unneglectable heterogeneity in quality and internal imbalance, and further verification of our prediction model may be necessary.

Radiomics consists of hundreds of possible valuable features, especially when frequency domain-related transformations are enabled. Meanwhile, complete clinical information and images are costly to collect. This phenomenon forms an imbalance between the rarity of clinical data and relatively easier-to-extend features. There are more features than samples, which creates difficulties for data mining. Therefore, the selection of radiomics features serves as the central section of the study, and understanding of each selected radiomics features is indispensable. First order, shape and even grey level derived matrices are constructed with exactly defined meanings. Thus, there could be simple mapping between these basic features and visible characteristics[8–10]. However, the majority of the selected features are wavelet features, which are based on frequency transformations, and filtering with wavelet functions is not directly appreciable. In digital image processing, the frequency domain has been proven to have

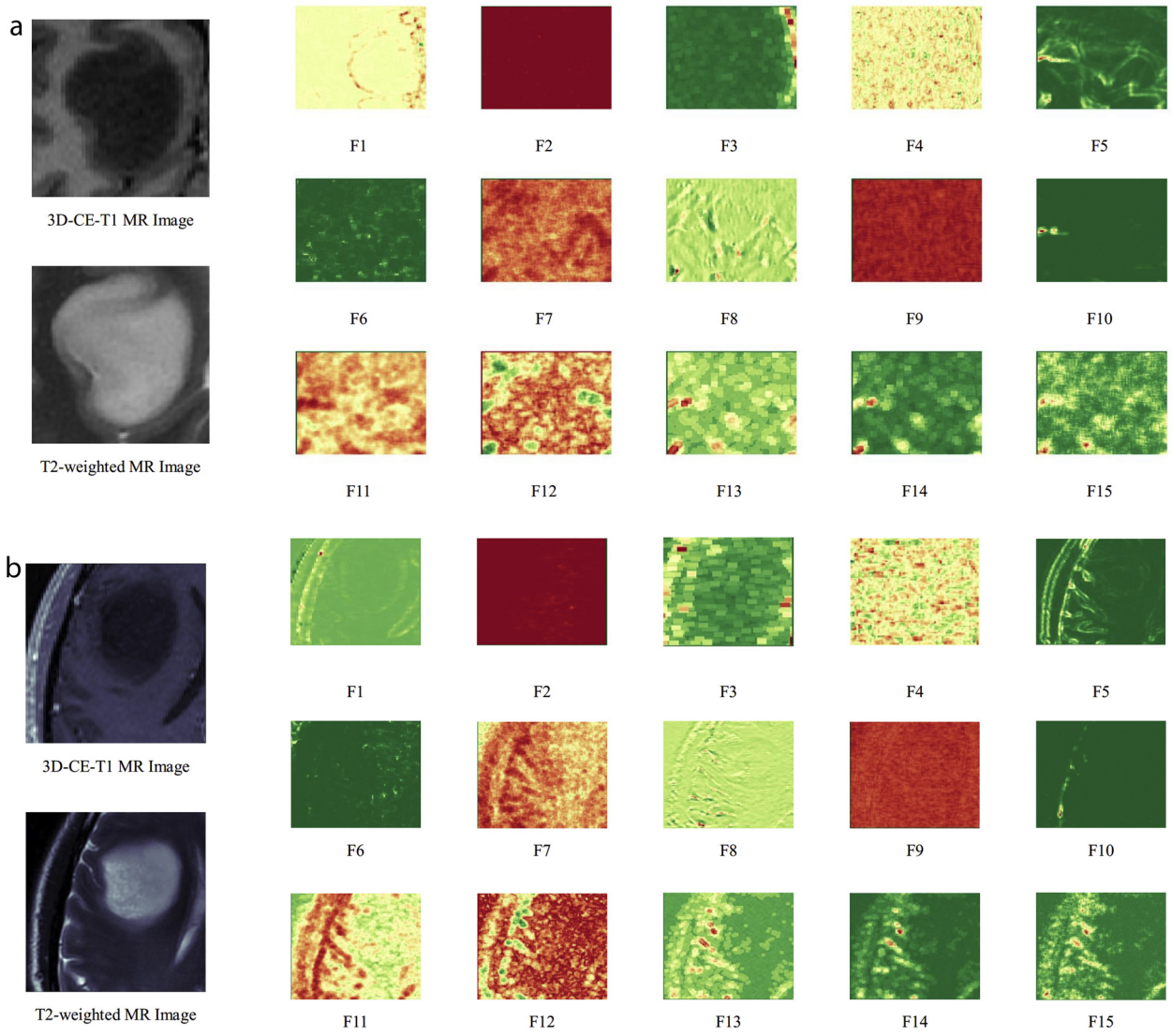

Fig. 3. The radiomics feature maps of the 15 selected features in the fusion radiomics model for an *MGMT* methylated patients (a) and *MGMT* unmethylated patients (b). The radiomics map was calculated with a 5 pixel * 5 pixel kernel which runs through the whole image, its radiomics features are labels as the values of the center of the covered area. For wavelet features, wavelet transforms are performed to three-dimensional space first. This method differs from what we calculated in the model, but it provides a time-efficient and intuitionistic way to visualize radiomics features.

important meaning for information carrying and depiction, and human vision also involves an imperceptible procedure of processing spatial-frequency information[35,36]. In this study, visualization of selected features helped us to better comprehend the information encompassed in the imaging data. The interpretation of the imaging features is meaningful no matter for studies using basic machine learning methods or using artificial neural networks. Not only does it specifically explain the radiographic differences between tumor phenotypes, but it may lead us to uncover the biological processes behind the imaging data and unveil new biomarkers which will have to be tested for clinical utility.

The performance of any of the single radiomics prediction models was not superior to that of the fusion radiomics model, nor was that of the linear combination. The fusion radiomics model performed better with a comparative quantity of features, indicating the importance of multi-modality images in the evaluation of gliomas. The coefficient of the linear combination exhibited a preference for T2-weighted images over 3D-CE-T1-weighted images, and same trend was also found in the composition of the fusion radiomics model. This observation is consistent with clinical experience that the T2-weighted images are primarily considered when evaluating nonenhanced tumors (predominantly LGGs among gliomas). However, the predictive values of the single T2 radiomics model and the linear radiomics model showed a group of samples which presented ambiguous probabilities near the classification threshold on both the training cohort and validation cohort, indicating that T2-weighted images can provide the model with the necessary information but lack some essential details. The missing details can be replenished by 3D-CE-T1-weighted features, and the incidences of boundary predictive values were decreased in the 3D-CE-T1-weighted single radiomics model and fusion radiomics model, suggesting that the radiomics features of 3D-CE-T1-weighted images are also indispensable when evaluating LGG even if there is no contrast enhancement (particularly in radiomics studies). In addition, although a linear combination is an easy and pragmatic algorithm that has advantages compared with different prediction models using single series imaging data, the performance of the linear combination model did not exceed that of the fusion model. With a fixed scale of the training cohort, stacking features together (e.g., the linear combination model) leads to the inclusion of more features than any single radiomics model, which may impede the convergence and statistical metrics of the model, while fusion feature selections provide with more relevant features with less redundant features.

Clinical factors such as patient age may influence *MGMT* promoter

methylation status[37]. In this study, patient age was not picked up by the LASSO selector in the clinical integrated model in the first 30 features with the highest potential contribution to the model. Further, age was appended as an additional feature to the selected radiomics features in the fusion model, while no visible increase in the model performance was observed. This result demonstrates that although clinical factors may be associated with the tumor phenotype (e.g., patient age may be associated with the *MGMT* promoter methylation status), clinical factors may not be the most significant characteristics for predicting the tumor phenotype compared to the selected radiomics features, and the addition of these clinical factors into the prediction model may increase the complexity without increasing the model performance.

When comparing the performance of the five radiomics models, the statistical advancement of the fusion and clinical integrated model was obvious for the training dataset, but the same significance was not achieved for the validation dataset. The Z-scores in the validation cohort was not high enough to demonstrate reliable differences, and the 95% confidence interval of the AUC exhibited a wide range, probably due to the limited scale of the validation dataset. Nevertheless, the fusion radiomics model showed the best performance and may be the most powerful model for predicting the *MGMT* promoter methylation status.

There might be overfitting problems in our model, regarding the high number of involving features. We construct an extra fusion radiomics model with 6 features: T1CE_wavelet-LHH_firstorder_Maximum, T1CE_wavelet-HHH_gldm_Small Dependence Low Gray Level Emphasis, T2_wavelet-LLH_glszm_Large Area High Gray Level Emphasis, T2_wavelet-LHH_firstorder_Median, T2_wavelet-HHH_glrlm_Run Variance, T2_wavelet-HHH_glszm_Size Zone Non Uniformity. The model achieve an AUC of 0.855(0.682-1.000) on the validation set. Besides, there is not significant statistical difference (P = 0.613) between the 6-feature and the original fusion radiomics model. Overfitting, a violation of parsimony, is not an absolute but involves a comparison[38]. For novel studies, the comparison was done between the model and the natural realities. Metrics on validation dataset were regarded as good indicators for the extent of overfitting, and the number of variables can also be empirical signals. The metrics of model was affected by the large heterogeneity in our validation dataset, which was a selected largest subset of the TCGA-LGG under our selection criteria. The extent of overfitting was indicated as acceptable with our new test on fusion radiomics model with simplified features indirectly.

The current study had several limitations. First, the differences in the methodology used to measure *MGMT* promoter status (e.g., pyrosequencing was performed for local samples, while a methylation chip was used for TCIA tissues) may have produced bias in the determination of *MGMT* status, despite the coherence assessment between techniques has been made[7]. Further large-scale studies with consistent *MGMT* evaluation techniques are essential to improve the performance of the prediction model. Second, the model was trained and validated without information regarding patients' prognosis because most of the patients did not meet their endpoint when the study was carried out, leaving the inability to prove its clinical significance. More comprehensive data that contain information on treatment and prognosis may be favorable for the implications of the radiomics model. Third, only conventional MRI images (3D-CE-T1 and T2-weighted images) were included in this study since they are the most appropriate sequences to locate and evaluate tumors in clinical practice. Alternative imaging sequences (e.g., perfusion-weighted MRI and diffusion-weighted MRI) may be further integrated into radiomics studies. In addition, segmentation of the ROI did not include peri-tumor areas which may also have glioma cell infiltration and contain information reflecting tumor phenotype. Finally, alternative histopathological and molecular markers (e.g., *IDH* mutations, chromosomal 1p/19q codeletion) also have considerable clinical significance and may be relevant to *MGMT* promoter methylation status[39], and further radiomics studies focusing on multiple tumor markers may increase the application prospects of radiomics investigation.

5. Conclusions

MRI-based radiomics models, especially the fusion radiomics model, could provide a reliable noninvasive method for the preoperative prediction of *MGMT* promoter methylation status in WHO grade II and grade III gliomas, allowing the potential for pretreatment prediction and personalized therapy for glioma patients.

Funding

This work was supported by the Chinese Academy of Medical Sciences Innovation Fund for Medical Sciences [grant number 2016-I2M-2-001], and the Fundamental Research Funds for the Central Universities [grant number 3332018029].

Declaration of Competing Interest

None.

Acknowledgement

The authors thank American Journal Experts for providing language help.

References

[1] S. Lapointe, A. Perry, N.A. Butowski, Primary brain tumours in adults, Lancet (London, England) 392 (10145) (2018) 432–446.
[2] M.E. Hegi, A.C. Diserens, T. Gorlia, M.F. Hamou, N. de Tribolet, M. Weller, J.M. Kros, J.A. Hainfellner, W. Mason, L. Mariani, J.E. Bromberg, P. Hau, R.O. Mirimanoff, J.G. Cairncross, R.C. Janzer, R. Stupp, MGMT gene silencing and benefit from temozolomide in glioblastoma, The New England journal of medicine 352 (10) (2005) 997–1003.
[3] E.H. Bell, P. Zhang, B.J. Fisher, D.R. Macdonald, J.P. McElroy, G.J. Lesser, J. Fleming, A.R. Chakraborty, Z. Liu, A.P. Becker, D. Fabian, K.D. Aldape, L.S. Ashby, M. Werner-Wasik, E.M. Walker, J.P. Bahary, Y. Kwok, H.M. Yu, N.N. Laack, C.J. Schultz, H.J. Gray, H.I. Robins, M.P. Mehta, A. Chakravarti, Association of MGMT Promoter Methylation Status With Survival Outcomes in Patients With High-Risk Glioma Treated With Radiotherapy and Temozolomide: An Analysis From the NRG Oncology/RTOG 0424 Trial, JAMA oncology (2018).
[4] W. Wick, C. Hartmann, C. Engel, M. Stoffels, J. Felsberg, F. Stockhammer, M.C. Sabel, S. Koeppen, R. Ketter, R. Meyermann, M. Rapp, C. Meisner, R.D. Kortmann, T. Pietsch, O.D. Wiestler, U. Ernemann, M. Bamberg, G. Reifenberger, A. von Deimling, M. Weller, NOA-04 randomized phase III trial of sequential radiochemotherapy of anaplastic glioma with procarbazine, lomustine, and vincristine or temozolomide, Journal of clinical oncology : official journal of the American Society of Clinical Oncology 27 (35) (2009) 5874–5880.
[5] T. Gorlia, M.J. van den Bent, M.E. Hegi, R.O. Mirimanoff, M. Weller, J.G. Cairncross, E. Eisenhauer, K. Belanger, A.A. Brandes, A. Allgeier, D. Lacombe, R. Stupp, Nomograms for predicting survival of patients with newly diagnosed glioblastoma: prognostic factor analysis of EORTC and NCIC trial 26981-22981/CE.3, The Lancet. Oncology 9 (1) (2008) 29–38.
[6] V. Quillien, A. Lavenu, M. Sanson, M. Legrain, P. Dubus, L. Karayan-Tapon, J. Mosser, K. Ichimura, D. Figarella-Branger, Outcome-based determination of optimal pyrosequencing assay for MGMT methylation detection in glioblastoma patients, Journal of neuro-oncology 116 (3) (2014) 487–496.
[7] P. Bady, D. Sciuscio, A.C. Diserens, J. Bloch, M.J. van den Bent, C. Marosi, P.Y. Dietrich, M. Weller, L. Mariani, F.L. Heppner, D.R. McDonald, D. Lacombe, R. Stupp, M. Delorenzi, M.E. Hegi, MGMT methylation analysis of glioblastoma on the Infinium methylation BeadChip identifies two distinct CpG regions associated with gene silencing and outcome, yielding a prediction model for comparisons across datasets, tumor grades, and CIMP-status, Acta neuropathologica 124 (4) (2012) 547–560.
[8] S. Drabycz, G. Roldan, P. de Robles, D. Adler, J.B. McIntyre, A.M. Magliocco, J.G. Cairncross, J.R. Mitchell, An analysis of image texture, tumor location, and MGMT promoter methylation in glioblastoma using magnetic resonance imaging, NeuroImage 49 (2) (2010) 1398–1405.
[9] J.A. Carrillo, A. Lai, P.L. Nghiemphu, H.J. Kim, H.S. Phillips, S. Kharbanda, P. Moftakhar, S. Lalaezari, W. Yong, B.M. Ellingson, T.F. Cloughesy, W.B. Pope, Relationship between tumor enhancement, edema, IDH1 mutational status, MGMT promoter methylation, and survival in glioblastoma, AJNR. American journal of neuroradiology 33 (7) (2012) 1349–1355.

[10] W.J. Moon, J.W. Choi, H.G. Roh, S.D. Lim, Y.C. Koh, Imaging parameters of high grade gliomas in relation to the MGMT promoter methylation status: the CT, diffusion tensor imaging, and perfusion MR imaging, Neuroradiology 54 (6) (2012) 555–563.
[11] P. Lambin, R.T.H. Leijenaar, T.M. Deist, J. Peerlings, E.E.C. de Jong, J. van Timmeren, S. Sanduleanu, R. Larue, A.J.G. Even, A. Jochems, Y. van Wijk, H. Woodruff, J. van Soest, T. Lustberg, E. Roelofs, W. van Elmpt, A. Dekker, F.M. Mottaghy, J.E. Wildberger, S. Walsh, Radiomics: the bridge between medical imaging and personalized medicine, Nature reviews. Clinical oncology 14 (12) (2017) 749–762.
[12] C. Hwan-Ho, P. Hyunjin, Classification of low-grade and high-grade glioma using multi-modal image radiomics features, Conference proceedings: Annual International Conference of the IEEE Engineering in Medicine and Biology Society. IEEE Engineering in Medicine and Biology Society. Annual Conference 2017 (2017) 3081–3084.
[13] C. De Looze, A. Beausang, J. Cryan, T. Loftus, P.G. Buckley, M. Farrell, S. Looby, R. Reilly, F. Brett, H. Kearney, Machine learning: a useful radiological adjunct in determination of a newly diagnosed glioma's grade and IDH status, Journal of neuro-oncology 139 (2) (2018) 491–499.
[14] J. Yu, Z. Shi, Y. Lian, Z. Li, T. Liu, Y. Gao, Y. Wang, L. Chen, Y. Mao, Noninvasive IDH1 mutation estimation based on a quantitative radiomics approach for grade II glioma, European radiology 27 (8) (2017) 3509–3522.
[15] Y.W. Park, K. Han, S.S. Ahn, S. Bae, Y.S. Choi, J.H. Chang, S.H. Kim, S.G. Kang, S.K. Lee, Prediction of IDH1-Mutation and 1p/19q-Codeletion Status Using Preoperative MR Imaging Phenotypes in Lower Grade Gliomas, AJNR. American journal of neuroradiology 39 (1) (2018) 37–42.
[16] H. Arita, M. Kinoshita, A. Kawaguchi, M. Takahashi, Y. Narita, Y. Terakawa, N. Tsuyuguchi, Y. Okita, M. Nonaka, S. Moriuchi, M. Takagaki, Y. Fujimoto, J. Fukai, S. Izumoto, K. Ishibashi, Y. Nakajima, T. Shofuda, D. Kanematsu, E. Yoshioka, Y. Kodama, M. Mano, K. Mori, K. Ichimura, Y. Kanemura, Lesion location implemented magnetic resonance imaging radiomics for predicting IDH and TERT promoter mutations in grade II/III gliomas, Scientific Reports 8 (1) (2018) 11773.
[17] P. Grossmann, D.A. Gutman, W.D. Dunn Jr., C.A. Holder, H.J. Aerts, Imaging-genomics reveals driving pathways of MRI derived volumetric tumor phenotype features in Glioblastoma, BMC cancer 16 (2016) 611.
[18] Z. Liu, Y. Wang, X. Liu, Y. Du, Z. Tang, K. Wang, J. Wei, D. Dong, Y. Zang, J. Dai, T. Jiang, J. Tian, Radiomics analysis allows for precise prediction of epilepsy in patients with low-grade gliomas, NeuroImage. Clinical 19 (2018) 271–278.
[19] H. Zhou, M. Vallieres, H.X. Bai, C. Su, H. Tang, D. Oldridge, Z. Zhang, B. Xiao, W. Liao, Y. Tao, J. Zhou, P. Zhang, L. Yang, MRI features predict survival and molecular markers in diffuse lower-grade gliomas, Neuro Oncol 19 (6) (2017) 862–870.
[20] P. Kickingereder, U. Neuberger, D. Bonekamp, P.L. Piechotta, M. Gotz, A. Wick, M. Sill, A. Kratz, R.T. Shinohara, D.T.W. Jones, A. Radbruch, J. Muschelli, A. Unterberg, J. Debus, H.P. Schlemmer, C. Herold-Mende, S. Pfister, A. von Deimling, W. Wick, D. Capper, K.H. Maier-Hein, M. Bendszus, Radiomic subtyping improves disease stratification beyond key molecular, clinical, and standard imaging characteristics in patients with glioblastoma, Neuro Oncol 20 (6) (2018) 848–857.
[21] Z.C. Li, H. Bai, Q. Sun, Q. Li, L. Liu, Y. Zou, Y. Chen, C. Liang, H. Zheng, Multiregional radiomics features from multiparametric MRI for prediction of MGMT methylation status in glioblastoma multiforme: A multicentre study, European radiology 28 (9) (2018) 3640–3650.
[22] Y.B. Xi, F. Guo, Z.L. Xu, C. Li, W. Wei, P. Tian, T.T. Liu, L. Liu, G. Chen, J. Ye, G. Cheng, L.B. Cui, H.J. Zhang, W. Qin, H. Yin, Radiomics signature: A potential biomarker for the prediction of MGMT promoter methylation in glioblastoma, Journal of magnetic resonance imaging : JMRI 47 (5) (2018) 1380–1387.
[23] J. Wei, G. Yang, X. Hao, D. Gu, Y. Tan, X. Wang, D. Dong, S. Zhang, L. Wang, H. Zhang, J. Tian, A multi-sequence and habitat-based MRI radiomics signature for preoperative prediction of MGMT promoter methylation in astrocytomas with prognostic implication, European radiology 29 (2) (2019) 877–888.
[24] M.J. van den Bent, H.J. Dubbink, M. Sanson, C.R. van der Lee-Haarloo, M. Hegi, J.W. Jeuken, A. Ibdaih, A.A. Brandes, M.J. Taphoorn, M. Frenay, D. Lacombe, T. Gorlia, W.N. Dinjens, J.M. Kros, MGMT promoter methylation is prognostic but not predictive for outcome to adjuvant PCV chemotherapy in anaplastic oligodendroglial tumors: a report from EORTC Brain Tumor Group Study 26951, Journal of clinical oncology : official journal of the American Society of Clinical Oncology 27 (35) (2009) 5881–5886.
[25] M.J. van den Bent, B. Baumert, S.C. Erridge, M.A. Vogelbaum, A.K. Nowak, M. Sanson, A.A. Brandes, P.M. Clement, J.F. Baurain, W.P. Mason, H. Wheeler, O.L. Chinot, S. Gill, M. Griffin, D.G. Brachman, W. Taal, R. Ruda, M. Weller, C. McBain, J. Reijneveld, R.H. Enting, D.C. Weber, T. Lesimple, S. Clenton, A. Gijtenbeek, S. Pascoe, U. Herrlinger, P. Hau, F. Dhermain, I. van Heuvel, R. Stupp, K. Aldape, R.B. Jenkins, H.J. Dubbink, W.N.M. Dinjens, P. Wesseling, S. Nuyens, V. Golfinopoulos, T. Gorlia, W. Wick, J.M. Kros, Interim results from the CATNON trial (EORTC study 26053-22054) of treatment with concurrent and adjuvant temozolomide for 1p/19q non-co-deleted anaplastic glioma: a phase 3, randomised, open-label intergroup study, Lancet (London, England) 390 (10103) (2017) 1645–1653.
[26] G. Reifenberger, B. Hentschel, J. Felsberg, G. Schackert, M. Simon, O. Schnell, M. Westphal, W. Wick, T. Pietsch, M. Loeffler, M. Weller, N. German Glioma, Predictive impact of MGMT promoter methylation in glioblastoma of the elderly, International journal of cancer 131 (6) (2012) 1342–1350.
[27] M. Jenkinson, C.F. Beckmann, T.E. Behrens, M.W. Woolrich, S.M. Smith, Fsl, NeuroImage 62 (2) (2012) 782–790.
[28] S.M. Smith, M. Jenkinson, M.W. Woolrich, C.F. Beckmann, T.E. Behrens, H. Johansen-Berg, P.R. Bannister, M. De Luca, I. Drobnjak, D.E. Flitney, R.K. Niazy, J. Saunders, J. Vickers, Y. Zhang, N. De Stefano, J.M. Brady, P.M. Matthews, Advances in functional and structural MR image analysis and implementation as FSL, NeuroImage 23 (Suppl. 1) (2004) S208–19.
[29] M.W. Woolrich, S. Jbabdi, B. Patenaude, M. Chappell, S. Makni, T. Behrens, C. Beckmann, M. Jenkinson, S.M. Smith, Bayesian analysis of neuroimaging data in FSL, NeuroImage 45 (Suppl. 1) (2009) S173–86.
[30] J.J.M. van Griethuysen, A. Fedorov, C. Parmar, A. Hosny, N. Aucoin, V. Narayan, R.G.H. Beets-Tan, J.C. Fillion-Robin, S. Pieper, H. Aerts, Computational Radiomics System to Decode the Radiographic Phenotype, Cancer Res 77 (21) (2017) e104–e107.
[31] J. Tang, S. Alelyani, H. Liu, Feature selection for classification: A review, Data classification: Algorithms and applications 37 (2014).
[32] F. Pedregosa, G. Varoquaux, A. Gramfort, V. Michel, B. Thirion, O. Grisel, M. Blondel, P. Prettenhofer, R. Weiss, V. Dubourg, J. Vanderplas, A. Passos, D. Cournapeau, M. Brucher, M. Perrot, E. Duchesnay, Scikit-learn: Machine Learning in Python, Journal of Machine Learning Research 12 (October) (2011) 2825–2830.
[33] J. Friedman, T. Hastie, R. Tibshirani, Regularization Paths for Generalized Linear Models via Coordinate Descent, J Stat Softw 33 (1) (2010) 1–22.
[34] E.R. DeLong, D.M. DeLong, D.L. Clarke-Pearson, Comparing the areas under two or more correlated receiver operating characteristic curves: a nonparametric approach, Biometrics 44 (3) (1988) 837–845.
[35] A. Cajar, R. Engbert, J. Laubrock, Spatial frequency processing in the central and peripheral visual field during scene viewing, Vision Res 127 (2016) 186–197.
[36] M.B. Sachs, J. Nachmias, J.G. Robson, Spatial-frequency channels in human vision, J Opt Soc Am 61 (9) (1971) 1176–1186.
[37] P. Mur, A. Rodriguez de Lope, F.J. Diaz-Crespo, T. Hernandez-Iglesias, T. Ribalta, C. Fiano, J.F. Garcia, J.A. Rey, M. Mollejo, B. Melendez, Impact on prognosis of the regional distribution of MGMT methylation with respect to the CpG island methylator phenotype and age in glioma patients, Journal of neuro-oncology 122 (3) (2015) 441–450.
[38] D.M. Hawkins, The problem of overfitting, J Chem Inf Comput Sci 44 (1) (2004) 1–12.
[39] P. Jha, V. Suri, A. Jain, M.C. Sharma, P. Pathak, P. Jha, A. Srivastava, A. Suri, D. Gupta, K. Chosdol, P. Chattopadhyay, C. Sarkar, O6-methylguanine DNA methyltransferase gene promoter methylation status in gliomas and its correlation with other molecular alterations: first Indian report with review of challenges for use in customized treatment, Neurosurgery 67 (6) (2010) 1681–1691.